

Magnetic phase separation and strong AFM nature of hexagonal Gd₅Sb₃

S. Shanmukharao Samatham,* Akhilesh Kumar Patel, and K. G. Suresh

Magnetic Materials Laboratory, Department of Physics,

Indian Institute of Technology Bombay, Mumbai 400076, Maharashtra, India

(Dated: November 10, 2017)

We report on the combined results of structural, magnetic, transport and calorimetric properties of Mn₅Si₃-type hexagonal Gd₅Sb₃. With decreasing temperature, it exhibits a ferromagnetic-like transition at 265 K, Néel transition at 95.5 K and a spin-orientation transition at 62 K. The system is found to be in AFM state down to 2 K in a field of 70 kOe. Magnetic phase coexistence is not noticeable despite large positive Curie-Weiss temperature. Instead low-temperature AFM and high-temperature FM-like phases are separated in large temperature. Temperature-magnetic field (H - T) phase diagram reveals field-driven complex magnetic phases. Within the AFM phase, the system is observed to undergo field-driven spin-orientation transitions. Field-induced tricritical and quantum critical points appear to be absent due to strong AFM nature and by the intervention of FM-like state between PM and AFM states. Electrical resistivity along with large Sommerfeld parameter suggests metallic nature.

I. INTRODUCTION

Gd-based compounds have been given due concern in the quest of large magnetocaloric effect (MCE). Various doping combinations have been tried ever since the discovery of large room temperature MCE in Gd. Later, R₅Ge₄ (R = Gd and M = Ge, Si) compounds have been recognized as promising MCE candidates with giant MCE (Gd₅Ge₂Si₂ [1, 2]), along with rich physical phenomena such as frozen magnetostructural first-order magnetic phase transition [3]. In recent times, belonging to the similar category but structurally different compounds R₅M₃ (M=Ge and Sb), are actively investigated for their interesting novel ground states [4–12]. Most of these compounds are found to crystallize in Mn₅Si₃-type hexagonal structure with P63/mcm (No. 193) space group [13]. The unit cell consists of five layers of atoms in c-axis direction. In this, R atom is located in two non-equivalent positions 4d (1/3, 2/3, 0) and 6g (x_R , 0, 0.25) whereas M atom is situated in 6g (x_M , 0, 0.25) position in which x_R and x_M are element specific. The low-temperature properties are reported to be affected mainly by the disorder caused by the presence of two non-equivalent sites of R atom; 6g and 4d. The interaction between the two layers (4d and 6g positions of R atom) plays an important role in determining the magnetic properties of these compounds.

Rare-earth antimonides R₅Sb₃ (R = Nd, Gd, Ho and Sm) have been reported to order antiferromagnetically with varying Néel temperatures (T_N), with an exception to La₅Sb₃ and Y₅Sb₃ [14]. Gd₅Sb₃ is reported to show paramagnetic (PM) to antiferromagnetic (AFM) transition around 110 K. Abdusalamov et al. reported complex magnetic structure of Gd₅Sb₃ [15] with Curie temperature $T_C \sim 260$ K, Curie-Weiss temperature $\theta_{CW} \sim 263$ K, effective magnetic moment $\mu_{\text{eff}} \sim 8.46/\text{Gd}^{+3}$ and

saturation moment $M_s \sim 32.5 \mu_B/\text{f.u.}$ (under 4.2 K and 200 kOe). Nagai et al. have reported three transitions at $T_C \sim 187$ K, $T_N \sim 100$ K and a ferrimagnetic transition below 50 K [11] with $\theta_{CW} \sim 266.8$ K and $\mu_{\text{eff}} \sim 10.9 \mu_B/\text{Gd}^{+3}$.

Manifestation of properties of the compounds that possess single magnetic phase transition such as PM-AFM or PM-FM, is somewhat predictable under the effect of external fields H . In either case, where T_N or T_C is suppressed by H down to $T = 0$, a quantum critical point is achieved. In a case where applied field induces the ferromagnetism, it leads to either metamagnetic (sudden) or spin-flop (gradual) transition. However, the scenario in compounds with multiple magnetic transitions is non-trivial in the sense that coexistence of phases leads to first order phase transition, zero-field ground state with weak AFM correlations leads to field-induced tricritical point etc.

The current study presents the detailed investigation of Gd₅Sb₃ using the combined results of structure, magnetization, specific heat and electrical resistivity. It shows temperature-driven multiple transitions from PM-FM (T_C), FM to AFM (T_C) and a low temperature spin-orientation like transition (T_t). The effect of magnetic field on these phases is discussed. Eventually, temperature-field (T - H) phase diagram, depicting field-induced magnetic changes in different magnetic phases, is presented.

II. EXPERIMENTAL METHODS

Polycrystalline Gd₅Sb₃ is prepared by arc melting the constituent elements (of purity at least 99.99%), taken in the stoichiometric ratio, under the inert Ar gas atmosphere. The ingot was remelted by flipping several times to ensure homogeneity. The weight loss during melting is less than 1%. The sample is annealed at 1273 K for seven days. X-ray diffraction pattern at room temperature is collected using PANalytical X'Pert PRO X-ray diffrac-

* sssrao@phy.iitb.ac.in

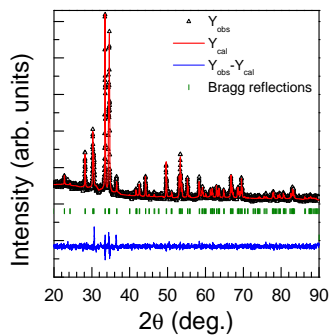


FIG. 1. Rietveld refined room temperature X-ray diffraction pattern of Gd_5Sb_3 . Experimental data shows good agreement with the generated pattern using $P63/mc$ space group. The estimated lattice parameters are $a(=b) \sim 9.02 \text{ \AA}$ and $c = 6.32 \text{ \AA}$.

TABLE I. Wyckoff positions of Gd_5Sb_3 after refinement

Position	Atom	x	y	z
4d	Gd	0.3333	0.6667	0
6g	Gd	0.24852	0	0.25
6g	Sb	0.61253	0	0.25

tometer on a powder specimen using $\text{Cu-K}\alpha$ radiation. The sample is found to be phase pure with no detectable traces of secondary phase, crystallizing in Mn_5Si_3 -type hexagonal crystal structure. Rietveld refinement of the same is shown in Fig. 1. Magnetization is measured using commercial Superconducting Quantum Interference Device-Vibrating Sample Magnetometer (SQUID-VSM). The measurements are carried out in isothermal and iso-field modes. Resistivity (by dc-linear four probe method) and specific heat (by relaxation calorimetric method) are carried out using 9 T/ 2 K - Physical Property Measurement System (Quantum Design).

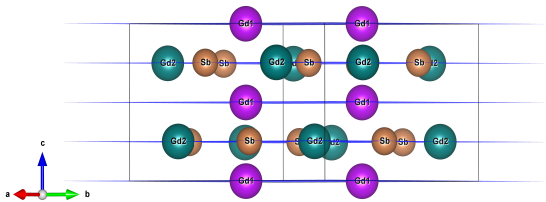


FIG. 2. The unit cell of Gd_5Sb_3 consisting of five layers along c -axis direction. Top, middle and bottom layers are with 4d (Gd_1) atoms and rest of the layers are occupied by 6g (Gd_2 and Sb) atoms.

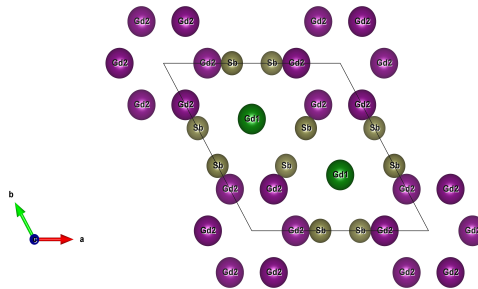


FIG. 3. ab -plane projection of unit cell with extended along corners for Gd_5Sb_3 .

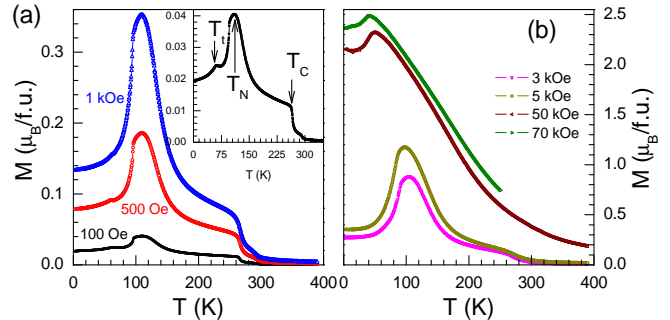


FIG. 4. Temperature dependence of magnetization of Gd_5Sb_3 in few representative magnetic fields. (a) $M(T)$ in 0.1, 0.5 and 1 kOe. The magnetic transitions are indicated by arrows (inset). T_N is observed to shift to low- T with H while T_C shifts to high- T .

III. RESULTS

Shown in Fig. 1(a) is the room temperature X-ray diffraction pattern along with the Rietveld refinement (using FullProf suit [16]) using space group $P63/mc$ (No: 193). The experimental intensities (Y_{obs}) are in excellent agreement with the generated intensities (Y_{cal}). The lattice parameters are $a(=b) \sim 9.02 \text{ \AA}$ and $c = 6.32 \text{ \AA}$ which are in good agreement with the previous reports [15, 17]. Table I shows the refined parameters along with atomic positions. Shown in Fig. 2 is the Gd_5Sb_3 unit cell. It comprises of five layers of atoms along the c -axis. Bottom, middle and top layers are occupied by 4d (Gd_1) positions and rest of the layers are filled with 6g (Gd_2 and Sb) positions. Fig. 3 shows the ab -plane projected view of Gd_5Sb_3 structure. The atoms are labeled as per the respective sites; Gd_1 at 4d, Gd_2 at 6g and Sb at 6g positions. At each corner, Gd_2 atoms form two opposite triangles (resembling hexagonal from top-view) with a side of $3.881(6) \text{ \AA}$. The nearest neighbor Gd_1 - Gd_1 (4d-4d) inter-atomic distance is 3.16 \AA and inter-layer Gd_2 - Gd_1 (6g-4d) inter-atomic distance is 3.80 \AA .

Figure 4 shows the temperature dependence of magnetization from 390 to 2 K, measured in zero-field cooled

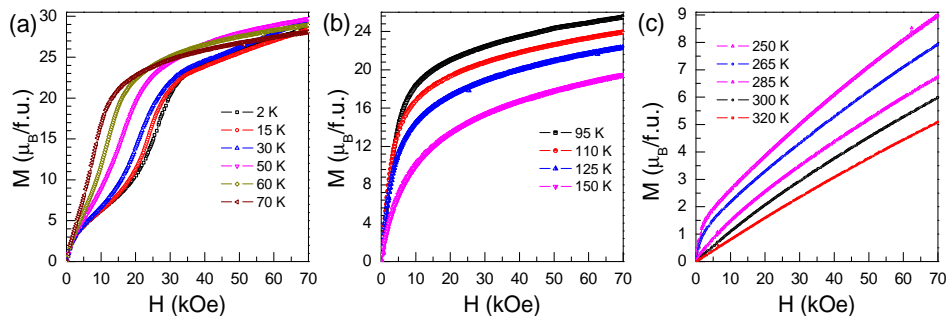


FIG. 5. Magnetization isotherms of Gd_5Sb_3 from 0 to 70 kOe, measured at labeled temperatures. (a) Below $T-t$ field-induced transition is noticed while (b) above T_N , ferromagnetic-like smooth increase of $M(H)$ is discernible. (c) At high temperatures i.e., in the paramagnetic region M goes linearly with H .

(ZFC) protocol, in few selected magnetic fields. Inset of Fig. 4(a) shows $M(T)$ in 100 Oe. Magnetization increases steeply below 400 K with a slope change at $T_C \sim 265$ K resembling ferromagnetic transition. After attaining a maximum around 100 K, magnetization falls rapidly below 95.5 K discerning an antiferromagnetic transition at T_N . In addition, a small peak around 62 K ($= T_t$) is noticed. It is observed that T_N -peak significantly increases and shifts to low-temperatures with increasing H while T_C shifts to high- T . T_t shifts to low- T by simultaneously smearing out. Shown in Fig. 5 are the magnetization isotherms $M(H)$ at few representative temperatures. A cursory look at the isotherms reveals that magnetization exhibits distinct field-driven phase crossovers at low temperatures up to 95 K. Between 95 K and 285 K, magnetization increases smoothly with H , similar to FM behavior. Almost linear increase of M with H is discernible above 285 K.

IV. DISCUSSION

Figure 6 shows the dc-susceptibility ($\chi_{dc} = M/H$) in 100 Oe from 390 to 310 K i.e., in the paramagnetic state. Curie-Weiss fit is used to estimate the effective moment (μ_{eff}) and Curie-Weiss temperature θ_{CW} .

$$\chi(T) = \frac{N_A \mu_{\text{eff}}^2}{3k_B(T - \theta_{\text{CW}})} \quad (1)$$

where N_A and k_B are the Avogadro's and Boltzmann constants, θ_{CW} is Curie-Weiss temperature. Thus estimated θ_{CW} and μ_{eff} are 223.5 ± 0.2 K and $3.71 \pm 0.7 \mu_B/\text{Gd}^{+3}$, respectively. Curie-Weiss temperature is large and positive which is in agreement with the literature [15]. However, the observed effective moment is smaller than that of Gd^{+3} free ion ($7.94 \mu_B$ with $J = 7/2$) and previously reported values $8.46 \mu_B/\text{Gd}^{+3}$ [15] and $10.9 \mu_B/\text{Gd}^{+3}$ [11]. While large positive Curie-Weiss temperature indicates the ferromagnetic correlations, the low effective moment may indicate the non-contribution of some of the Gd moments by screening effects. Suppression of

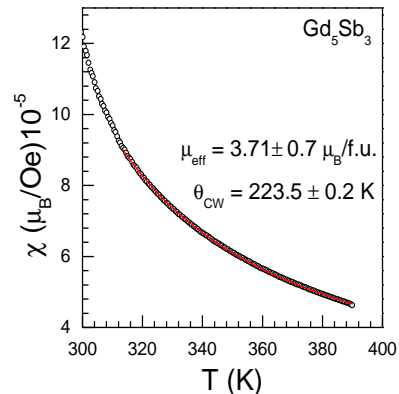


FIG. 6. Temperature dependence of dc-susceptibility $\chi_{dc}(T)$ in 100 Oe. A fit of Curie-Weiss law Eq. 1 in the paramagnetic region yields a θ_{CW} of about 224 K and effective moment of about $3.7 \mu_{\text{eff}}/\text{f.u.}$

the moment due to crystal field is also ruled out as it is Gd. In addition, $M(T)$ measurements are also performed in field-cooled cooling (FCC) and field-cooled warming (FCW) modes. No considerable hysteresis between FCC and FCW curves is observed, ruling out the first order behavior between high- T FM-like to low- T AFM phases.

In order to understand the magnetic states in Gd_5Sb_3 , it is worth knowing various types of phenomena resulting from the competing magnetic interactions. The resultant depends on not only the strength of interactions but also the nature of high- and low- T magnetic phases. In most of the rare-earth based compounds, generally one comes across two types of magnetic phases *viz.*, AFM and FM and a competition between them. For instance, we discuss the types of magnetic phenomena in compounds with dual transitions and no phase coexistence. First let us consider the case with a transition from high- T AFM to low- T FM phase. With increasing H , FM transition is shifted to high- T while that of AFM phase is shifted to low- T . Apparently, with increasing magnetic field strength, two simultaneous processes occur; stabilization of low- T FM at high temperatures and suppression of AFM phase to low temperatures (an otherwise

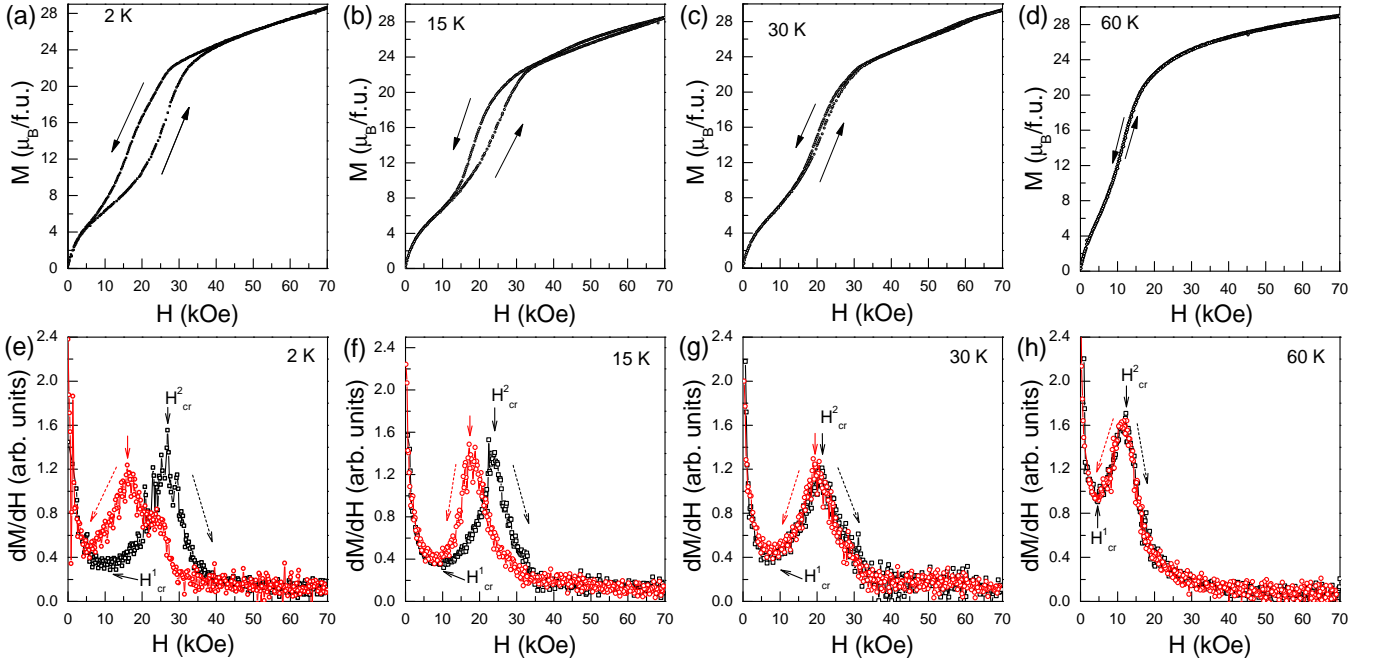


FIG. 7. (a-d) Magnetization isotherms of Gd_5Sb_3 measured in increasing and decreasing magnetic fields at few representative temperatures and (e-h) their corresponding dM/dH plots. Below spin orientation temperature ($T_t \sim 62$ K), the compound shows field-induced hysteresis loop, shown in dM/dH as two distinct peaks in red hallow circles and black hallow squares.

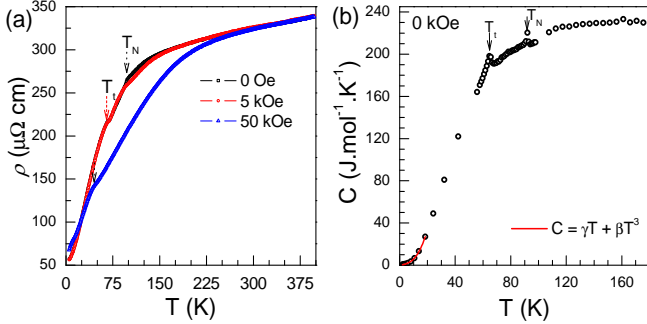


FIG. 8. Temperature variation of (a) resistivity and (b) specific heat. The dual transitions T_N and T_t are indicated by arrows. Specific below 20 K is fitted to the equation $C = \gamma T + \beta T^3$ and the estimated Sommerfeld parameter is about $215 \text{ mJ.mol}^{-1}.\text{K}^{-1}$.

extension of PM phase to low temperatures). As a result, the zero-field thermal separation $\Delta T (= |T_N - T_C|)$ between the phases is reduced in finite fields. In other words, thermal ($k_B \Delta T$) and magnetic (μH) energies act cooperatively with each other and consequently establish FM state by ceasing the high- T AFM phase in relatively low-fields. The temperature and field at which PM-AFM transition ceases to exist allowing a continuous PM-FM transition is generally noted as field-induced tricritical point.

The scenario is just the opposite in the case of a transition from high- T FM and low- T AFM phase. With

increasing field strength, T_C and T_N continue to increase in opposite temperature directions. Low- T AFM phase is suppressed to further low temperatures and high- T FM phase is expanded to low temperatures at the cost of AFM phase. Zero-field ΔT increases with field. As a result, $k_B \Delta T$ and μH oppose each other, requiring high magnetic fields to stabilize FM phase down to the lowest temperature. Nevertheless, the compounds (for example Gd_3Co [18] and PrCuSi [19]) undergoing a transition from PM to AFM with prevailing FM correlations in the paramagnetic limit (identifiable by positive θ_{CW}) are found to be unstable against applied H . The weakly correlated AFM phase is susceptible to H and eventually converts to FM phase in presence of relatively low fields. However, irrespective of the nature of high- and low- T magnetic phases, in the context of phase-coexistence (AFM and FM) phenomena the properties are governed by the competing interactions of AFM and FM magnetic clusters formed in zero-field. Applied H tries to break the antiferromagnetically interacting clusters, leading to FM phase growth. Such a scenario may either lead to first-order kinetic arrest or second-order spin glass states [20].

Now, we attempt to understand the magnetic scenario of Gd_5Sb_3 . As seen in the Figs. 4(a&b), Gd_5Sb_3 belongs to the latter case with high- T FM-like and low- T AFM. The separation of phases in temperature is noticeable from the increase of T_C and decrease of T_N . To know more about the magnetic nature of the compound, magnetization isotherms are measured in five quadrants

($0 \rightarrow H_{\max} \rightarrow 0 \rightarrow -H_{\max} \rightarrow 0 \rightarrow H_{\max}$). For clarity, only first quadrant is shown in Fig. 5, for magnetizing and demagnetizing fields since the positive and negative quadrants are found to be symmetric. At 2 K, two field-driven transitions are observed at $H_{\text{cr}}^1 \sim 11.4$ kOe and $H_{\text{cr}}^2 \sim 26.7$ kOe. H_{cr}^2 is attributed to AFM to high moment FM-like spin-flop transition whereas H_{cr}^1 is a spin-reorientation transition. No saturation is observed up to 70 kOe. Variations of H_{cr}^1 and H_{cr}^2 with temperature are represented by plotting dM/dH vs. H , Figs. 7(e-f). The hysteresis between H_{cr}^1 and H_{cr}^2 is perceptible from the low H_{cr}^2 in decreasing fields (peak at 15.98 kOe represented by red hallow circles). The non-saturation of $M(H)$ is because of an incomplete transformation of AFM phase at 2 K, as shown in $M(T)$ the λ -type Néel transition at 37.6 K. With increasing temperature (i.e., moving towards T_N), H_{cr}^1 and H_{cr}^2 decrease monotonically, suggesting the ceasing of field-driven phase transition and hysteresis simultaneously at T_N . Further, above T_N , a smooth increase of M with H is observed, which is in consonance with the ferromagnetic-like behavior between $T_N \leq T \leq T_C$.

Further to understand the transport and calorimetric behavior, electrical resistivity and specific heat of Gd_5Sb_3 are measured. Shown in Fig. 8(a) is the temperature dependence of resistivity $\rho(T)$ from 2-375 K in a few representative fields, 5 and 50 kOe. The system is metallic down to 2 K with a residual resistivity ρ_0 of about $48 \mu\Omega\text{cm}$. Relatively large residual resistivity ratio ($\rho_{300\text{K}}/\rho_0 \simeq 7$) implies the good quality of the prepared polycrystalline sample. Zero-field $\rho(T)$ shows kinks at T_N and T_t . In agreement with the $M(T)$ measurements, magnetic field suppression of the transitions is observed in field-resistivity curves. Figure 8(b) depicts specific heat $C(T)$ from 2-285 K, showing T_N and T_t respectively at 92 K and 65 K. $C(T)$ is fitted using the equation $C = \gamma T + \beta T^3$ for $T \leq 20$ K. The estimated Sommerfeld coefficient $\gamma \sim 215 \text{ mJ}\cdot\text{mol}^{-1}\cdot\text{K}^{-1}$, implying the metallic character. Debye temperature $\theta_D \sim 161$ K.

Temperature-magnetic field (T - H) phase diagram is shown in Fig. 9, which is constructed on the basis of field-variation of T_C and T_N along with temperature-variation of critical fields H_{cr}^1 and H_{cr}^2 . FM and AFM regions are separated in temperature. With increasing fields, FM expands to low- T by suppressing AFM phase. The system is observed to undergo two spin-reorientation transitions at 2 K within 30 kOe. However, it is noticed that higher fields are required to completely suppress the AFM state down to 2 K. The system avoids field-induced tricritical and quantum critical points are due to strong AFM characteristics and by the intervention of FM-like state between PM and AFM phases.

As mentioned earlier, no thermal hysteresis between FCC and FCW curves in the temperature range $T \in [T_C, T_N]$ discards the temperature-driven first order phase transition in Gd_5Sb_3 . Despite large positive Curie-Weiss temperature, FM and AFM phases are found not to co-exist. Instead, the magnetic phases are thermodynamically

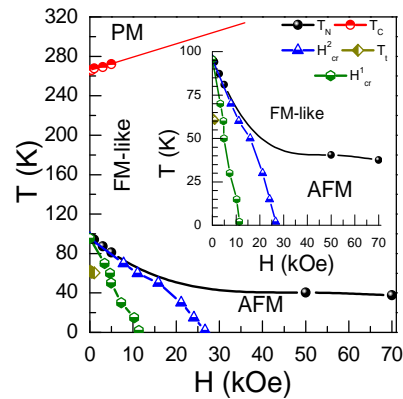


FIG. 9. Temperature-field (T - H) phase diagram of Gd_5Sb_3 , showing paramagnetic (PM), ferromagnetic (FM)-like and AFM phases with decreasing temperature. T_C increases with field whereas T_N decreases. Solid red is guide to an eye. Inset: field-induced dual transitions in AFM region using H_{cr}^1 and H_{cr}^2 boundaries. T_t boundary ends at 3 kOe.

separated in zero field. A rough estimation of magnetic field needed to bring full FM nature at low temperatures is estimated by equating thermal energy $k_B\Delta T$ with $\mu_{\text{eff}}H$. For Gd_5Sb_3 , with $\Delta T = 170$ K, $H \sim 684$ kOe is required to overcome the thermal energy barrier. However, at room temperature, the field required to saturate the magnetization is estimated to 1200 kOe. J value, reverse calculated using $\mu_{\text{eff}} = 2\sqrt{J(J+1)} = 3.7 \mu_B/\text{Gd}^{+3}$, is close to $3/2$. However, magnetic state below Néel temperature is complex in character and needs further attention. Initially, at 2 K, it undergoes field-driven dual transitions from canted to AFM and AFM to spin-flop state within external fields of 70 kOe.

V. CONCLUSION

In conclusion, we report on the combined results of structural, magnetic, transport and calorimetric properties of Gd_5Sb_3 . It crystallizes in Mn_5Si_3 -type hexagonal crystal structure. AFM and FM-like phase are separated in large temperature. It exhibits field-driven complex magnetic phases. No magnetic phase coexistence is observed. Large Sommerfeld coefficient and positive temperature coefficient of resistivity suggest metallic nature. Within the AFM phase, the system is observed to undergo field-driven spin-orientation transitions. Field-induced tricritical and quantum critical points appear to be absent due to the strong AFM nature and by the intervention of FM-like state between PM and AFM states. In order to reveal the complex magnetic structure of Gd_5Sb_3 , magnetization measurements in high (pulsed) fields along with neutron diffraction measurements as a function of temperature are highly desirable.

ACKNOWLEDGMENTS

The authors acknowledge IRCC and Department of Physics for the magnetization, specific heat and resis-

tivity facilities. SSS is supported by Indian Institute of Technology Bombay Institute Post Doctoral Program.

-
- [1] V. K. Pecharsky and K. A. Gschneidner, Jr., *Phys. Rev. Lett.* **78**, 4494 (1997).
- [2] K. A. Gschneidner Jr, V. K. Pecharsky, and A. O. Tsokol, *Reports on Progress in Physics* **68**, 1479 (2005).
- [3] L. S. Sharath Chandra, S. Pandya, P. N. Vishwakarma, D. Jain, and V. Ganesan, *Phys. Rev. B* **79**, 052402 (2009).
- [4] P. Kushwaha and R. Rawat, *Solid State Communications* **152**, 1824 (2012).
- [5] B. Maji, K. G. Suresh, and A. K. Nigam, *J. Phys.: Condens. Matter* **23**, 506002 (2011).
- [6] B. Maji, K. G. Suresh, X. Chen, and R. V. Ramanujan, *Journal of Applied Physics* **111**, 073905 (2012).
- [7] B. Maji, K. G. Suresh, and A. K. Nigam, *Europhys. Lett.* **91**, 37007 (2010).
- [8] R. Nirmala, A. V. Morozkin, A. K. Nigam, J. Lamsal, W. B. Yelon, O. Isnard, S. A. Granovsky, K. K. Bharathi, S. Quezado, and S. K. Malik, *J. Appl. Phys.* **109**, 07A716 (2011).
- [9] T. Tsutaoka, A. Tanaka, Y. Narumi, M. Iwaki, and K. Kindo, *Physica B* **405**, 180 (2010).
- [10] D. A. Joshi, A. Thamizhavel, and S. K. Dhar, *Phys. Rev. B* **79**, 014425 (2009).
- [11] M. Nagai, A. Tanaka, Y. Haga, and T. Tsutaoka, *Journal of Magnetism and Magnetic Materials* **310**, 1775 (2007).
- [12] V. Svitlyk, F. Fei, and Y. Mozharivskyj, *Journal of Solid State Chemistry* **181**, 1080 (2008).
- [13] K. H. J. Buschow and J. F. Fast, *physica status solidi (b)* **21**, 593 (1967).
- [14] J. Yakinthos and I. Semitelou, *Journal of Magnetism and Magnetic Materials* **36**, 136 (1983).
- [15] M. Abdusaljamova, V. Abulchaev, R. Levitin, A. Markosijan, V. Popov, and R. Yumaguzhin, *Journal of the Less Common Metals* **120**, 281 (1986).
- [16] J. Rodriguez-Carvajal, *Physica B: Condensed Matter* **192**, 55 (1993).
- [17] W. Rieger and E. Parthè, *Acta Cryst. B* **24**, 456 (1968).
- [18] S. S. Samatham, S. Barua, and K. G. Suresh, *Journal of Magnetism and Magnetic Materials* **444**, 439 (2017).
- [19] A. M. Strydom, *The European Physical Journal B* **74**, 9 (2010).
- [20] S. B. Roy and M. K. Chattopadhyay, *Phys. Rev. B* **79**, 052407 (2009).